Thermally and electrically conductive multifunctional sensor based on epoxy/graphene composite

Han, S., Chand, A., Araby, S., Cai, R., Chen, S., Cheng, R., Kang, H. & Meng, Q.

DOI 10.1088/1361-6528/ab5042
ISSN 0957-4484
ESSN 1361-6528

Publisher: IOP Publishing

Mechanically strong, thermally and electrically conductive multifunctional sensor based on epoxy/graphene composite

Sensen Han[1,2], Aron Chand[1], Sherif Araby[1,3,4*], Rui Cai[5], Shuo Chen[6], Hailan Kang[7], Rongqiang Cheng[1], Qingshi Meng[1,2*]

[1] College of Aerospace Engineering, Shenyang Aerospace University, Shenyang 110136, China

[2] Shenyang Aircraft Design Institute, Shenyang 110136, China

[3] Department of Mechanical Engineering, Benha Faculty of Engineering, Benha University, Benha, Egypt

[4] School of Engineering, University of South Australia, SA, 5095, Australia

[5] School of Mechanical, Aerospace and Automotive Engineering, Coventry University, Coventry, UK

[6] School of Sino-Dutch Biomedical and Information Engineering, Northeastern University, Shenyang 110819, Liaoning, China

[7] School of Materials Science and Engineering, Shenyang University of Chemical Technology, Shenyang, China

[*]Corresponding Authors：Sherif Araby: SherifAraby.Gouda@unisa.edu.au

Qingshi Meng; Email: mengqingshi@hotmail.com

Abstract

Flexible electronics is expected to be one of the most active research areas in the next decade. In this study, a mechanically robust, flexible and durable epoxy/GnP composite film was fabricated having percolation threshold of electrical conductivity at 1.08 vol% GnPs with high thermal conductivity as 1.47 W m^{-1} K^{-1} at 10 vol% GnPs. The composite film shows high mechanical performance: Young's modulus and tensile strength were improved by 1344% and 66.7%, respectively at 10 vol%. The film has demonstrated high sensitivity to various mechanical loads: (i) it gives good electrical response at high bend and torsion angles up to 180°; and (ii) it displays a good compressive load response up to 2N where the absolute value of electrical resistance change increased by 71%. Furthermore, the film has showed an excellent reliability up to 5.5×10^3 cycles with maintaining zero-point error. Above 20 ºC, the film solely acts as a temperature sensor; upon cyclic temperature testing, the film demonstrated a stable resistive response in the range of 30 −75 ºC. This flexible composite film has remarkable properties that enable it to be used as a full-fledged sensor for universal applications in aerospace, automotive and civil engineering.

Key words: Graphene; Epoxy; Electrical and thermal conductivity; Strain; Sensor

1. Introduction

Recently, high-performance flexible multifunctional polymer composite films have attracted extensive attention in both academia and industries for potential applications in automobile, energy, bio-health monitoring and communication industries [1, 2]. When polymers are combined with electrically and/or thermally conductive nanofillers, a polymeric nanocomposite films featuring thin, lightweight, flexible, wearable, and electric and thermal properties are developed. These developed composites could have potential in sensing signals depending on the attained features.

Strain sensors refer to a class of electronic devices, which transduce mechanical deformations into electrical signals. They are highly desirable in wearable devices to record human physical motions for therapy and health condition monitoring such as heart rate monitoring. Soft stretchable strain sensors are increasingly demanded to measure movement on stretchable and curved surfaces (wrist patch on skin) and the developed hoop strain on curved pressure vessels.

Polymers are intrinsically poor in electrical and thermal conductivity. Adding a conductive phase (fillers) into the polymeric matrix is one way to develop conductive polymer composites. The host polymer is transformed into conductive material when the concentration of the conductive phase exceeds the percolation threshold where the conductive fillers overlap and contact each other throughout the matrix. Another mechanism to understand the conduction behavior in a polymeric composite is through tunneling-transfer mechanism where the conductive nanofillers are very close but not touching each other; minimum distance between two conductive fillers to observe tunneling effect is 1.8 nm [3].

Various conductive materials including metal nanostructures (gold nanoparticles, gold and silver nanowires) [4-6] and carbon-based nanomaterials – graphene [7, 8] and carbon nanotubes (CNTs)[9-

11]–, and carbon black [12] – were investigated to develop multifunctional polymer-based composite films. Metal-based sensors normally have poor stretchability and undesirable heavy weight due to its high density [13]. Graphene is highly electrically and thermally conductive material with outstanding mechanical properties: specific surface area 2630 m^2 g^{-1}, Young's modulus ~1 TPa, tensile strength ~130 GPa and electrical conductivity up to 6000 S/cm which are close to those of CNTs [14]. *Graphene platelets (GnPs) are few graphene layers (~3) stacked together with an average thickness of 3.55±0.32nm [15, 16]. In our previous work, GnPs were fabricated by thermal shocking graphite intercalated compound (GIC) at 700°C following by ultrasonication [16, 17]. GnPs proved to markedly enhance mechanical, electrical and thermal properties of various types of polymers when they added into them [16-18].*

Polymeric composite films and sensors developed using carbon nanotubes and graphene, possess light weight, flexibility, stretchability and promising sensitivity and durability compared to metallic nanoparticles. Plethora studies have investigated the structure-property relations of polymer/graphene and CNT nanocomposites and films [3, 19-26]. The minimum concentration of CNTs in a polymer needed to reach percolation threshold (φ_{th}) was theoretically calculated suggesting that only 3.33% of CNTs contribute to the conductive network at φ_{th} [20]. This is mainly because CNTs have high attractive force (van der Waal force) over tube surface leading to agglomeration and bundling inside the matrix. Also, it is important to mention that polymer properties, nanofiller conductivity and its structure characteristics, dispersion quality, and processing conditions are key factors in determining the composite-based sensor behavior [21, 22].

Lubineau G. et al [3] modified multi-walled CNT (MWCNT) by coating them with a conductive polymer, poly(3,4-ethylenedioxythiophene)poly(styrenesulfonate), and added to polycarbonate

matrix. The electrical resistivity was dropped by 11 orders when 1 wt% of modified MWCNT added compared to 8 orders when pristine MWCNTs were added at the same fraction. This confirms the crucial role of high degree of filler dispersion that was attained by modification via coating with conductive polymer. However, the piezoresistive response was deteriorated upon coating. The piezoresistive phenomena is one of the outstanding property of MWCNTs which makes them ideal candidate to develop polymer-based strain sensors [24]. Gau C. et al [25] succeeded in developing a promising pressure sensor composite containing polyimide and MWCNTs. The composite possessed highly linear piezoresistive and rapid response, high sensitivity and thermal stability which make the developed sensor competitive to a commercial pressure sensor. Hu N. et al. [21] developed epoxy/CNT based strain sensors with gauge factor (sensitivity) up to 25. They also emphasized that higher tunneling resistance can raise the sensitivity of the composite sensor. In recent study [27], epoxy/graphene platelet strain sensor was developed possessing a gauge factor of 22.54. Initially, the sensors were only applicable for strain sensing [28, 29]. However, with advancement in technology and fabrication methods, the sensors now have the ability to detect other parameters such as exposure to gas [30], ability to detect pressure [31] and photo sensing [32].

Most of previous studies develop nanocomposite which focuses on sensing one parameter–unifunctional sensor–especially strain sensing [33, 34]. Limited studies have been conducted on developing epoxy/GnP-based sensor which has the potential to simultaneously detect multiple parameters (pressure, temperature and strain). Hence, this research stands out from other previous work in developing an efficient and multifunctional sensor based on epoxy/GnP nanocomposite.

In this work, a mechanically strong, flexible and highly conductive (electrically and thermally) epoxy/GnP composite film sensor is fabricated. It is not only limited to sensing strain, but also able

to respond to angular movement. The developed sensor has high reliability with zero-point error since it lasts to work effectively up to 5.5×10^3 *cycles. Additionally, Our composite film can efficiently work as a temperature sensor at range 30–70℃.*

2. Experiment details

2.1 Material

The expandable graphite (graphite intercalation compound, GIC, *Asbury* 1721) was provided by *Asbury Carbons, Asbury, NJ, USA*. Epoxy – (diglycidyl ether of bisphenol A; WSR618, 184–200 g per equiv.) was purchased from Nantong Xingchen Synthetic Material. The hardener, Jeffamine D-2000 (J2000) was purchased from Huntsman, China.

2.2 Fabrication of composite film

The preparation of GnPs is fully described elsewhere [35]. In brief, 1 g GIC was expanded by transferring it into a preheated crucible at 700℃ in a common furnace; after 1 min, the crucible was taken out and cooled down. The expansion ratio of GIC calculated ~200 times by volume [16, 36]. A determined weight of the expanded GIC was then suspended in acetone at 1 wt% in a metallic container using a magnetic stirrer for 10 min followed by 1 hour ultrasonication below 20℃; the low temperature of ultrasonication enhances the delamination and suspension of the expanded GIC [37]. Upon completion of sonication, the end-product is graphene platelets (GnPs) [17, 35, 38]. The mixture will be used for the following preparation of epoxy/GnP composite film.

Epoxy resin was added and mixed with GnPs/acetone suspension by magnetic stirrer for 10 min to reach dissolving. The hardener–J2000 was slowly added to the epoxy/GnPs and manually stirred using a glass bar. The entire mixture was then sonicated for 30 min at room temperature and then *sat*

on a hot plate at 70℃ with magnetic stirring till approximately 70% (by volume) of acetone was evaporate. The mixing and evaporation processes were performed in a Pyrex Griffin beaker, 500ml and 1000ml. The remained mixture was dropped into a polypropylene mould and left for 12 hrs at room temperature producing semi-cured film and meanwhile the remaining acetone is evaporated. The semi-cured film is transferred to an oven at 120℃ for 8 hours for full curing and removing any traces of acetone. The fabrication process is summarized schematically in Figure 1. It is noteworthy to mention that all composite constituents were weighed in order to achieve a certain volume percentage. Equation 1 was used to convert weight percent to volume percent where density of epoxy and GnPs are defined as 1.1 and 2.26 g/cm^3 , respectively [36].

$$V_f = \frac{\rho_m w_f}{\rho_f(1 - w_f) + \rho_m w_f} \qquad Eq.1$$

where ρ and w are the density and weight fraction, respectively; subscript m refers to epoxy and hardener together, and f refers to GnPs.

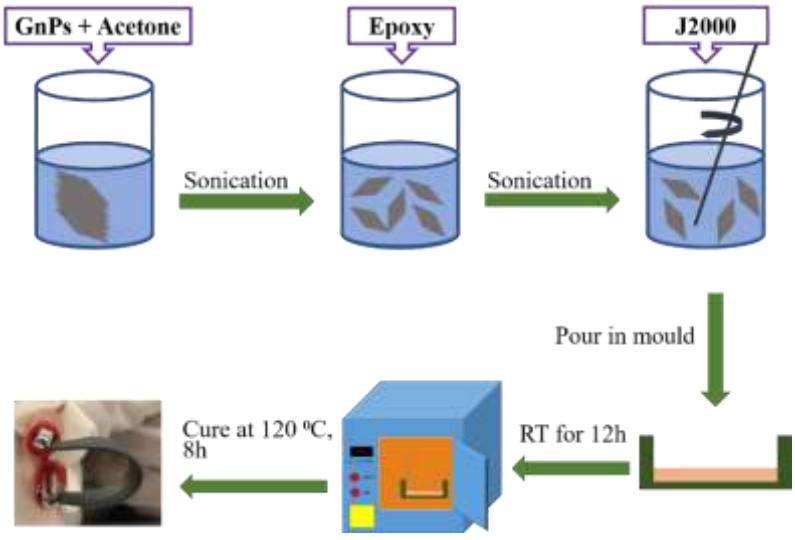

Figure 1. The fabrication process of epoxy/GnP composite film.

2.3 Characterizations

Transmission electron microscopy (TEM) Philips CM200, was used to study the microstructure of

graphene platelets (GnPs) at 200 kV accelerating voltage. The samples were prepared by dispersing graphene platelets into acetone via sonication with a subsequent dilution until it reaches concentration of 0.0004 wt%. Few drops of the 0.0004 wt% were dropped on 200-mesh copper grids then dried. The microstructure of the composite films was examined using scanning electron microscopy (SEM) (JEOL JSM-7800F) at 5 kV accelerating voltage. *A thin layer of platinum was used to coat the surface of the sample. Raman Spectra was collected using Renishaw inVia Raman spectrometer and 633nm laser excitation.*

Graphene platelet (GnP) powder was produced as follow. After the expanded GIC was ultrasonicated for one hour in acetone, the acetone was separated from the sonicated mixture using vacuum filtration. The wet product left overnight in a ventilated oven at 70°C to completely remove any traces of the solvent. The produced powder is GnP powder. To measure the intrinsic electric conductivity of GnP-sheet, GnP powder was pressed using bench-top hydraulic press to form a thin sheet of overlapped GnPs with thickness of ~ 0.5mm. Four-probe method was used to measure the in-plane electrical conductivity by commercial DC four-probe resistance measuring apparatus (RTS-8, 4 PROBES TECH Co., Ltd., China). The four probes were gently pressed onto the sheet to acquire good contact. The probes were by default separated ~1mm distance. The four-probe method determines the sheet resistance as R_s (Ω/□). The bulk conductivity is calculated according to Eq.2 [39]

$$\sigma\ (S/cm) = \frac{1}{R_s(\Omega/\square) \times t(cm)} \qquad Eq.2$$

where σ and t are respectively the bulk conductivity and sheet thickness. The measuring current was set at 1 mA, DC. The measurement was repeated over three prepared sheets and bulk resistivity was averaged.

The through-plane electrical volume resistivity of the developed epoxy/GnP composite was measured using Agilent 4339B high-resistivity meter connected with a 16008B resistivity cell. The volume resistivity measurement was performed in accordance to *ASTM D257-99*. *The Agilent resistivity meter was set at 5V and the electrical current was DC type.* Three measurements were conducted for each fraction to obtain the average. Each sample is 5±1.1 mm in thickness and 26 ± 0.5 mm in diameter. The thickness of the composite was measured by a digital micrometer.

Thermal conductivity of the composite was measured using TA Instruments DTC300 analyzer. The test samples were placed between the upper and lower heating plates where the temperature difference is 30°C. The lower plate is part of the calibration heat flowmeter. An axial temperature gradient is developed when the heat transferred from the upper plate through sample to lower plate. The test was in accordance with the *ASTM E1530* standard.

The piezoresistive property is the change of the electrical resistance of a material upon applying mechanical strain. The piezoresistive performance of the composite film was evaluated by conducting different types of mechanical loads including compressive, tensile, torsion, bending and thermal strains. The corresponding electrical resistance change in all mechanical loads was recorded using a FLUKE 2638A data acquisition system at current source and electrical potential of 100 μA and 12 V, respectively. Details of the applied mechanical thermal loads are described as follows.

Mechanical properties and piezoresistive property of the composite film under tensile loading were measured using a quasi-static uniaxial tensile test. It was carried out using a universal tensile testing machine (*XIANGMIN) equipped with 2 kN load cell and run* at cross-head speed 0.5 mm/min. *Stress-strain curves were plotted using the collected data and thus Young's modulus, tensile strength and elongation at break were determined*. The test was replicated five times for each fraction. *The recoded*

mechanical properties are the average values. While the tensile testing was running, the change in electrical resistance was determined. Two identical-copper wires attached to the composite film by silver past and the other ends of the wires are connected to FLUKE data-acquisition system to simultaneously record the resistance change upon tensile strain.

The piezoresistive response of the composite film upon compressive strain was performed using a manual hydraulic press. Pressure was exerted upon the film by placing it between two flat surfaces, the upper surface is manually moved till touching the film surface at which the pressure is 0. Then the pressure was step-wisely increased to 2N with 0.5N increment. Similar to tensile test, the film was connected to a FLUKE data-acquisition system to simultaneously record the resistance change with pressure increment at room temperature.

Thermal strain was applied over the epoxy/GnP composite film by placing the composite film inside a program-controlled temperature medium. The temperature range was programmed to work from --20 to 110 °C at a rate of 5 °C/min. The resistance was monitored using the FLUKE data acquisition unit. However, we noticed that resistance does not change much at temperature range -20–20°C. Therefore, the plotted data are from room temperature to 110°C.

Durability and reliability of the epoxy/GnP film was determined by fatigue test. It was conducted under tensile load mode using the universal tensile testing machine (XIANGMIN) equipped with 2 kN load cell. The fatigue test was performed within strain rage 0–5% at frequency of 1 Hz. The cyclic loading was carried out for 10,000 cycles. The resistance across the specimen during cyclic testing was monitored using FLUKE data acquisition unit. Figure 2. Summarizes fabrication process and piezoresistive measurements carried out over the 10 vol% epoxy/GnP composite film.

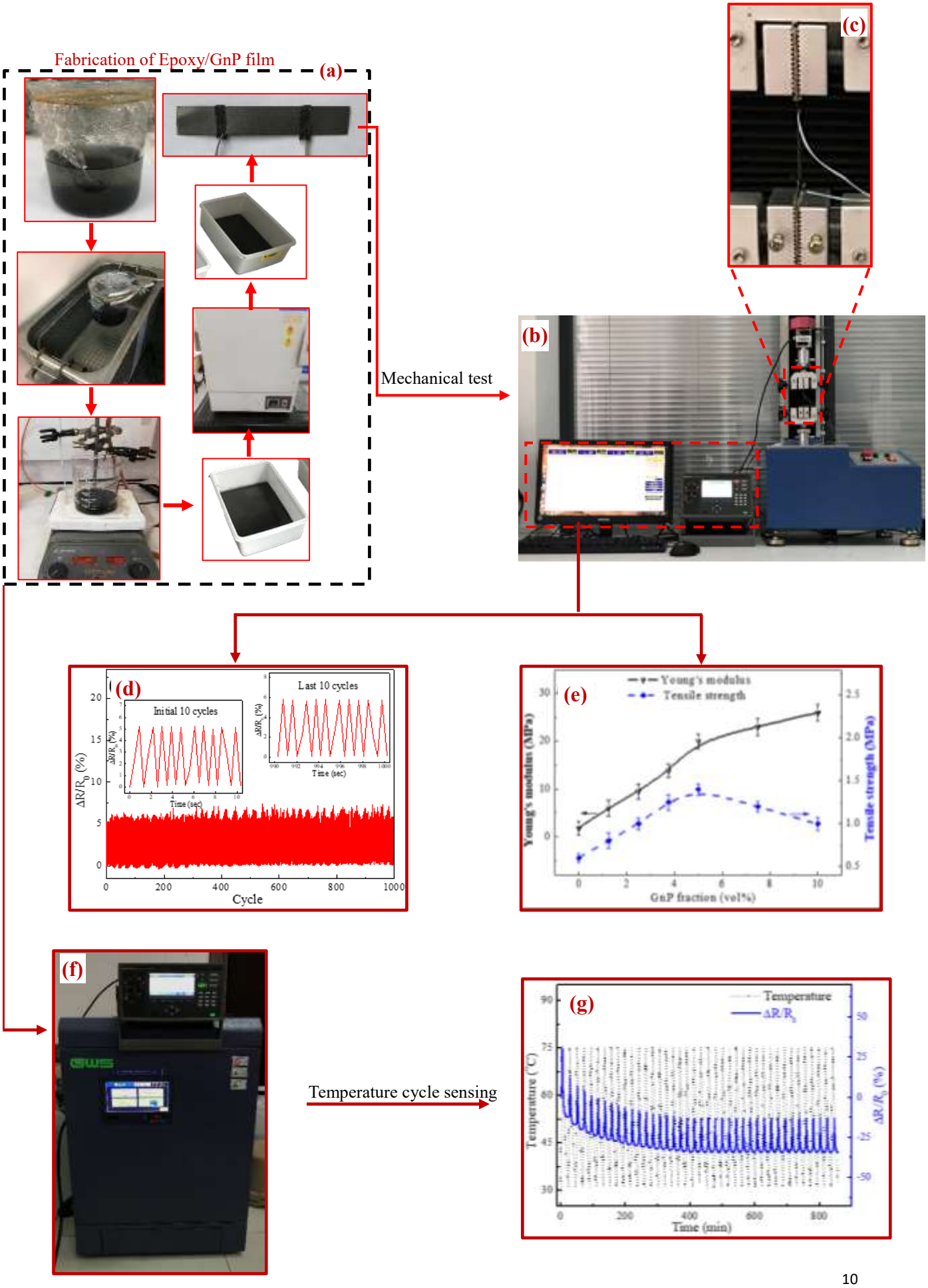
Fabrication of Epoxy/GnP film
(a)
(b)
(c)
Mechanical test
(d)
Initial 10 cycles
Last 10 cycles
Time (sec)
ΔR/R0 (%)
Cycle
(e)
Young's modulus
Tensile strength
Young's modulus (MPa)
Tensile strength (MPa)
GnP fraction (vol%)
(f)
Temperature cycle sensing
(g)
Temperature
ΔR/R0
Temperature (°C)
ΔR/R0 (%)
Time (min)

Figure 2. Complete digital-photo chart representing fabrication and measurement processes

3. Result and discussion

3.1 Morphology of graphene platelets

Transmission electron microscopy

Figure 3a–c shows the representative morphology of the GnPs. In image (a) giant piece of plate-like structure is found, they are layers of graphene stacked together. When part of the layer is magnified in image (b), edges of individual layers are observed confirming that our GnP might compromise of ~ 5 layers. Some other areas are bright and featureless (red circle) which mean this area contains one or two layers. Also, the blue arrows show the common wrinkled morphology of the thermally produced graphene in image (b). A randomly selected area at red circle was selected to study the electron diffraction (ED) pattern. Image (c) contains a typical highly crystalline structure of graphene.

Raman Spectroscopy

The graphitic structure and surface integrity of graphene platlets were studied and compared to graphite intercalation compounds (GIC) by Raman spectroscopy as shown in Figure 3d. The absorptions of D, G and 2D bands of GnPs were observed at 1360, 1580 and 2723cm^{-1}, respectively confirming the graphitic characteristics of the synthsiesed GnPs. Similar absorptions were noticed for GIC with marginal shifts. In graphene, the intensity of the D-band refers to in-plane sp^3 hybridized carbon structure associating with quantity of the disordered structure and defects such as vacancies due to oxidation and reduction, and grain boundries. On the other hand, G-band corresponds to the ordered structure of sp^2- hybridized carbon atoms. Thus, the I_D/I_G ratio quantifies the degree of structural integrity of GnPs which was calculated as 0.08 compared to ~1.0 in case of reduced graphene oxide [35]. This indicates our GnPs possess high structural integrity reflecting high

electrical conductivity and mechanical performance. The I_D/I_G ratio of GIC (0.25) depicts that our starting material has fair structural integrity with low oxidation degree yielding GnPs with high structural integrity. Since the synthsiesed GnPs possess more than 4 layers, it is difficult to distinguish its 2D-band from graphite [40, 41]. However, the GnPs' thickness was confirmed by atomic force microcopy in our previous studies [17, 36, 38, 42].

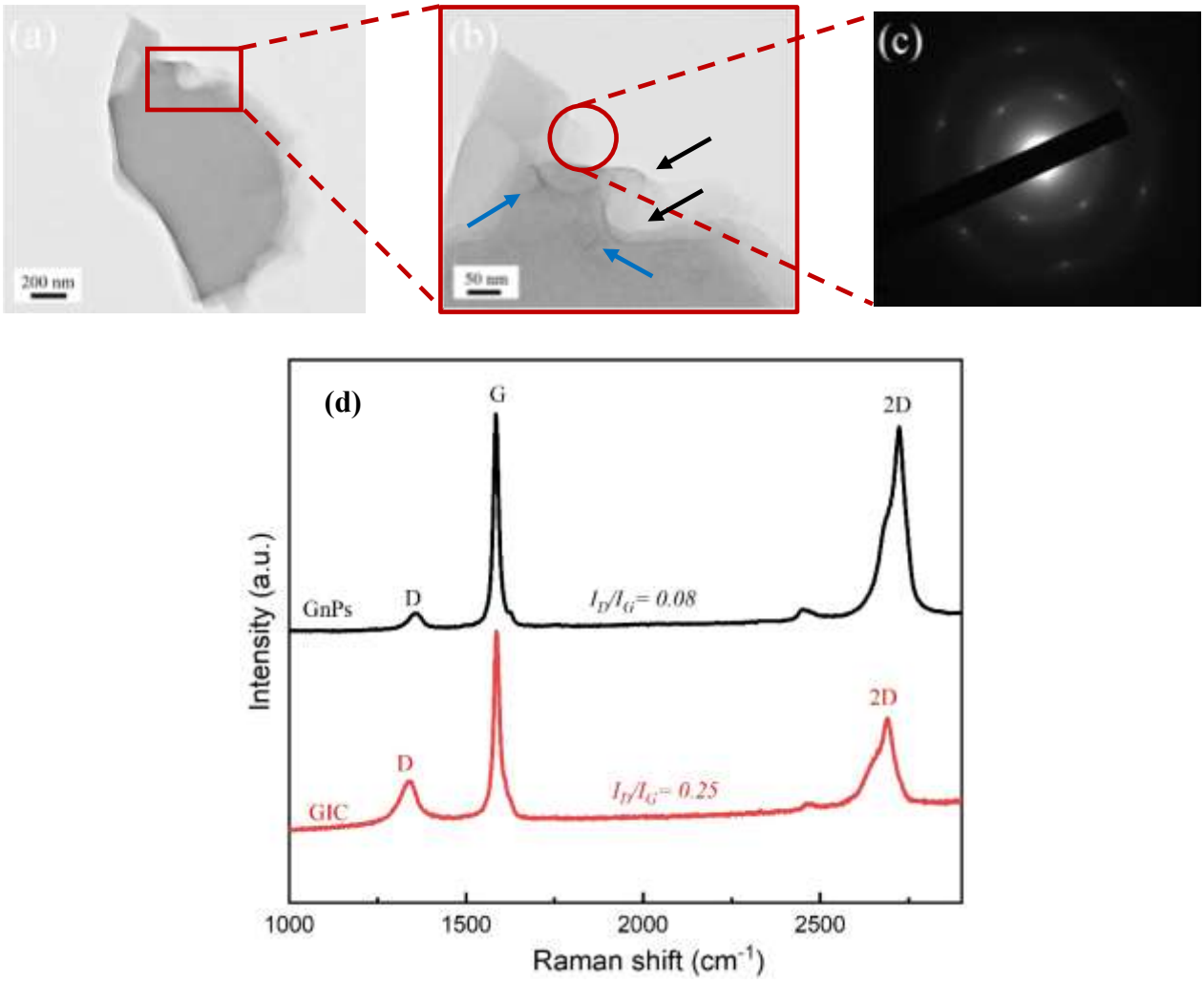

Figure 3. (a,b) TEM images of GnPs, (c) electron diffraction pattern selected from the red circle, *and (d) Raman Spectra of graphene platelets (GnPs) and graphite intercalation compounds (GIC)*

3.2 Electrical conductivity of GnPs

The intrinsic electrical conductivity of graphene platelet sheet recorded 1460 S/cm using the four-probe method and Eq.2. For comparison, the electric conductivity of a monolayer graphene produced

by chemical vapor deposition is 2000 S/cm [43]. Due to the overall high contact resistance between the overlapped sheets, the GnP electrical conductivity is lower than that of monolayer graphene. However, GnP electrical conductivity is far higher than that of graphene oxide (0.05 S/cm), chemically reduced graphene oxide (5 S/cm) or thermally reduced graphene oxide (350 S/cm) [44]. This indicates that GnPs have high surface integrity with less lateral defects. Taking into account the scalable production of GnPs and its cost-effectiveness, little difference with conductivity of monolayer graphene and the absolute non-conductive nature of most polymers, GnPs are promising fillers to develop electrically conductive polymer composites at low cost.

3.3 Composite films properties

Electrical conductivity of the composite films

In this study, GnPs have substantially enhanced the electrical conductivity of the epoxy composites. *At low fractions of GnPs, the composites are expected to have high volume resistivity. Therefore, the electrical volume conductivity of composites containing GnP in range 0 –3 vol% was measured by Agilent 4339B high-resistivity meter displayed in Figure 4a as a function of GnP vol%. Figure 4a displays that epoxy conductivity does not substantially change within the low fractions (vol%<0.75%). Once the GnP content is beyond 1 vol%, the electric conductivity of epoxy/GnP composite exponentially increases transforming the epoxy matrix from non-conductive material into a semi-conductive one whose inherited from the intrinsic superb electrical conductivity of GnPs.* For example, the electrical conductivity of neat epoxy augmented from 10^{-14} to 10^{-7} S/cm at 3 vol% recording 7 orders increase. Putting the measurements into the power low equation (Eq.3) gives more understanding when the percolation threshold is formed [17, 45].

$$\sigma_c = \sigma_f \ (\varphi - \varphi_t)^t \qquad \text{Eq. 3}$$

where σ_c, σ_f are respectively the composite and filler conductivities, and φ, φ_t are the filler content and percolation threshold in vol%, respectively; t is the critical exponent. The calculated percolation threshold value for the epoxy/GnP composite film was at ~1.08 vol%. At this fraction, a connected global network of GnPs was formed inside the epoxy matrix facilitating the electrons mobility across the matrix and breaking its nonconductive behavior.

When the fraction of GnPs increases beyond 3 vol%, the composite has high electrical conductivity and thus Agilent 4339B high-resistivity meter was not suitable to measure the composite conductivity. A four-probe method was employed to record the surface resistivity then using Eq.1 to convert it into bulk conductivity as presented in Figure 4b. After surpassing percolation threshold, the electrical conductivity linearly and steadily increased with GnP vol% due to the multitude of conductive phase creating numerous conductive passes across the composite. For example, at 10% vol of GnPs, the epoxy composite possesses electrical conductivity of ~0.01 S/cm, recording an increase by 11 order of magnitude compared to neat epoxy.

Thermal conductivity of the composite films

Thermal conductivity of epoxy/GnP composite films was studied at different levels of GnP vol%. Thermal conductivity measurements and enhancement percentage are shown in Figure 4c. The results revealed that the thermal conductivity rises steadily and linearly with the addition of GnPs. For example, the thermal conductivity of composite reached 1.47 W m^{-1} K^{-1} at 10 vol% GnPs recording 819% improvement compared to neat epoxy.

Thermal conductivity mainly relies on phonon transfer *via* lattice vibration. Neat polymers usually scatter the phonons when they transfer from one side to another due to nonconnected chain structure of polymers. When GnPs are added, phonons have better paths to pass with lower scattering compared

to the neat polymer. However, the Kapitza resistance; thermal resistance at interface between filler and matrix (GnP and epoxy); highly affects the overall thermal conductivity of the composite *[46-48]*. This explains the linear augment in thermal conductivity compared to the percolation behavior in electrical conductivity.

Mechanical performance of the composite films

Young's moduli and tensile strengths of neat epoxy and its composite films are depicted in Figure 4d. Obviously, adding GnPs into epoxy has a significant influence on the mechanical performance of the composite film. With the increase of GnP content, the Young's modulus and tensile strength of the composite film exhibit a prominent enhancing trend. For example, at 10 vol% GnP, the Young's modulus and tensile strength reached 26 ± 1.7 MPa and 1.0 ± 0.08 MPa, demonstrating 1344% and 66.7% improvement respectively, compared to the neat epoxy proving successful reinforcement of epoxy matrix by GnPs.

However, it is noticed that tensile strength trend inflected at 5 vol% GnP. Initially, the tensile strength increased to 1.4 ± 0.07 MPa at 5 vol% GnP and then decreased to 1 ± 0.08 MPa at 10 vol%, demonstrating an increment of 133.3% at 5 vol% and then reduction by 28.6% at 10 vol%. Similar trend was reported by Meng, Q et al. [49] where the increase in tensile strength was due to: (i) uniform dispersion of nanofillers and (ii) strong mechanical interlocking between the filler and matrix. These factors are more effective at low filler fraction hence resulting in high tensile strength. The noticed drop in tensile strength after 5 vol% GnP is due to the toughening and stiffening effect of the matrix upon introducing a stiff nanofiller (Young's modulus of graphene is ~ 1TPa). Figure 4(e) shows the elongation at break decreases upon filler addition, emphasizing that the matrix is undergoing stiffening effect. Similar results were reported by Ma J et al. [50]. Based on the revealed mechanical properties, electrical and thermal conductivity, the composite with 10 vol% GnPs was chosen in order

to study its piezoelectric performance.

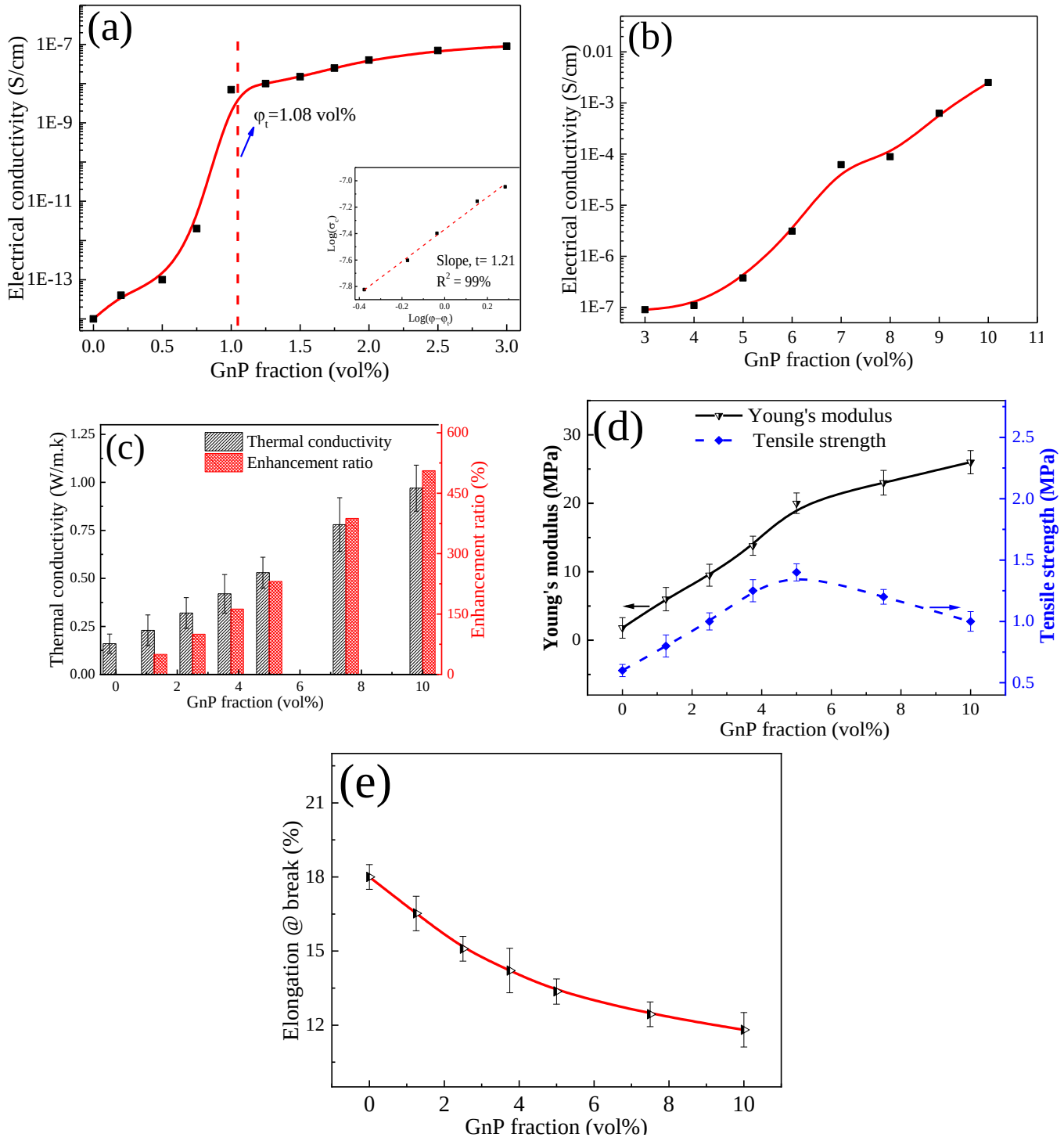

Figure 4. Functional and mechanical properties of epoxy/GnP composite film: (a,b) electrical percolation threshold and conductivities at different filler fraction, (c) thermal conductivity, (d) Young's modulus and tensile strength, and (e) elongation at break

3.3 Morphology of epoxy/GnP composite film

Since microstructure of neat epoxy is featureless and possesses a smooth cross-section surface structure [51], its SEM image is not presented here. The SEM micrographs for epoxy/GnP at 5 vol%

(Figure 5a1–a4) and 10 vol% (Figure 5b1–b4) were presented in order to show changes in microstructure with the progress of GnP content. At both contents, GnPs generally show relatively uniform dispersion with good mechanical interlocking with the matrix leading to high mechanical stiffness.

At low fraction 5 vol%, Image (a1) shows sponge-like microstructure displaying micropores throughout the cross-section with rough surface due to the breakage of GnP flakes. When the micrograph is magnified to Image (a2 & a3), giant GnPs are overlapped and tightly connected to each other leading to a conductive epoxy/GnP composite (~3×10^{-7} S/cm at 5 vol%). This supports the observed percolation threshold at 1.08 vol%. Image (a4) presents sharp and rough edge of GnP which enhance the mechanical interlocking with the matrix leading to high stiffness and maximum tensile strength –Figure 4d.

At high fraction, 10 vol%, microstructure images show dense and compact structure of GnPs over the entire cross-section. However, few small micropores are presented in Images (b2–b4) (blue circles). The compact structure does not allow much epoxy to penetrate into GnPs networks, nonetheless the 5 vol% structure does. Also, at high volume fractions, small quantity of bonding phase (epoxy) is available leading to relatively weak interface between the matrix and GnPs compared to 5 vol%; epoxy works as bonding material between GnPs and matrix as the same time. Consequently, the composite is not able to resist the mechanical deformation once the applied stress is beyond the yield point, demonstrating lower tensile strength compared to 5 vol%. However, Young's modulus increases with the GnP fraction because it is calculated at the elastic region.

Apart from mechanical performance, the multitude of GnPs in the matrix at high fractions provides several conductive paths throughout the matrix recording electrical conductivity of ~0.01 S/cm at 10 vol% GnPs.

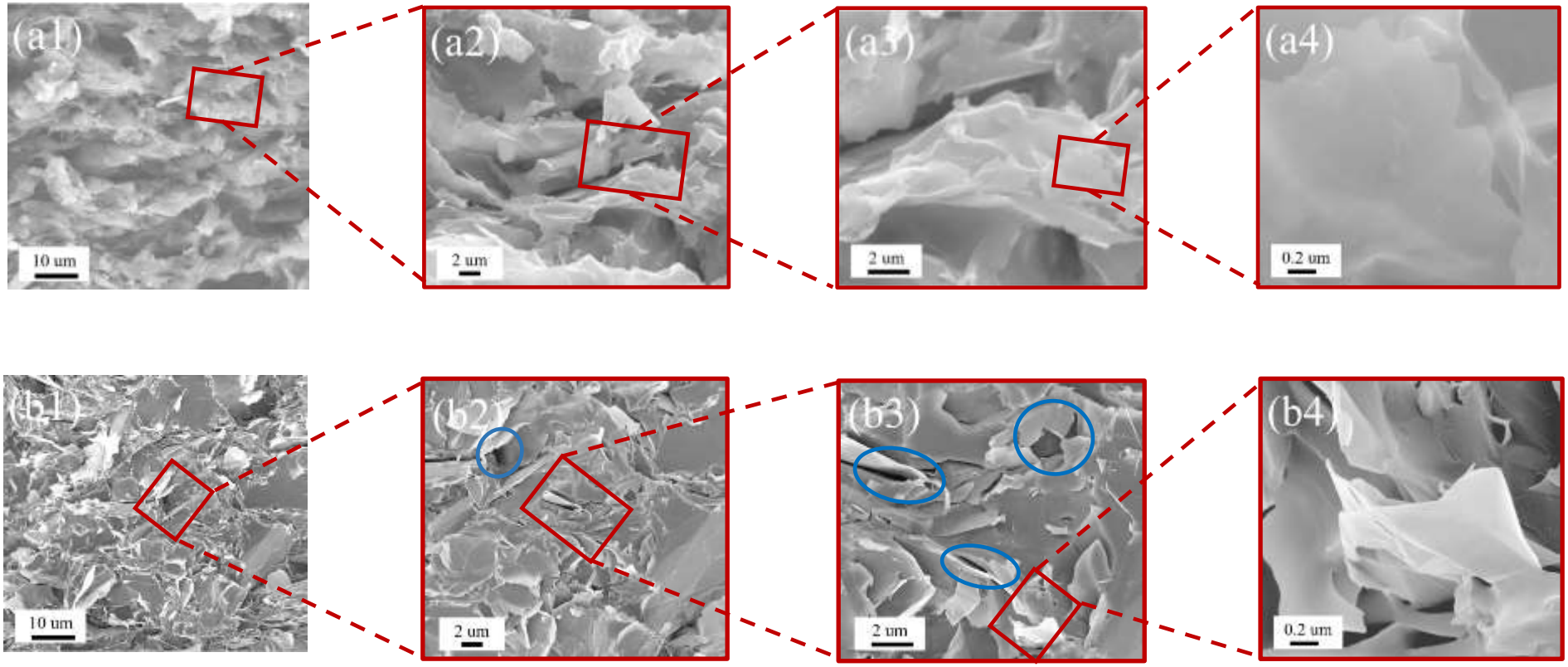

Figure 5. SEM images of epoxy/GnP composite films; (a1-a4) 5 vol% GnP content and (b1-b4) 10 vol% GnP content

3.4 Flexible Sensing

In this section, 10 vol% GnP composite film was used to *examine its piezoresistive performance under various dynamic engineering applications. In the discussion below, the resistance change refers to ΔR=R-R₀ and relative resistance change is ΔR/ R₀ where R are the measured film resistance corresponding to the stimulating signal and Ro is the film resistance at zero signal (zero strain for instance). Gauge factor is calculated as:*

$$GF = \frac{\Delta\ (\Delta R/R_o)}{\Delta\varepsilon} \qquad \textit{Eq. 4}$$

Figure 6a shows the relative change in resistance as a function of strain. *Since tensile strain is one of the most important mechanical deformation, it was thoroughly studied. It is observed that the relative resistance change in Figure 6a can be divided into two linear segments; first one is from 0 to 7 % strain and the second is within strain range 7–10 %. At range 0–7%, strain sensitivity (gauge factor)is calculated as 2 while at the second range the gauge factor is 6 which are the slopes of the fitting lines presented in the insets. These results tell that the film is able to sense and distinguish between low and high strain affecting a structure. The change in sensitivity of the composite film at low and high strains is due to (i) at low strain range, the overlap and connection between graphene platelets is firm and thus resistance does not change much resulting in low gauge factor ,2, and (ii) at high strain, some of the network branches are broken and disconnected, increasing the overall resistance of the composite leading to gauge factor of 6 .*

Figure 6b–d shows that the developed epoxy/GnP film is able to detect not only tensile strain but various mechanical deformations including compression, bending and torsion. Figure 6b shows relative resistance change of the composite film at various compressive loads. When the compressive load augments to 2N, the value of |ΔR/R₀| increased from 0 to 71%. This result demonstrates that the composite film has high sensitivity to compressive loads and is able to sense loads as small as 0.01N. Under compressive load, the distance *between adjacent graphene sheets planes within the composite film decreases resulting in better connection between GnPs in the 3D network paths.* This would lead

to a decrease in the composite's electric resistance and ultimately an increase in absolute value of *relative resistance change.* This gives our sensor the ability to work as a load cell with high resolution. Figure 6c shows electrical response of the composite film as a function of bending angle. The composite film could be bent up to 180º, demonstrating a good flexibility. With the bending angle increasing to 180º, the $\Delta R/R_0$ increased from 0 to 45%. *This may be due to the fact that the distance between GnPs at the bend increases as the bending angle increases, which makes the sensing ability more pronounced.*

Figure 6d shows the linear dependence of the $\Delta R/R_0$ with the angle of torsion. The composite film was twisted by 180º, which demonstrates an excellent flexibility within this range (0–180º). With the torsional angle increasing to 180º, the $\Delta R/R_0$ increased from 0 to 30%.

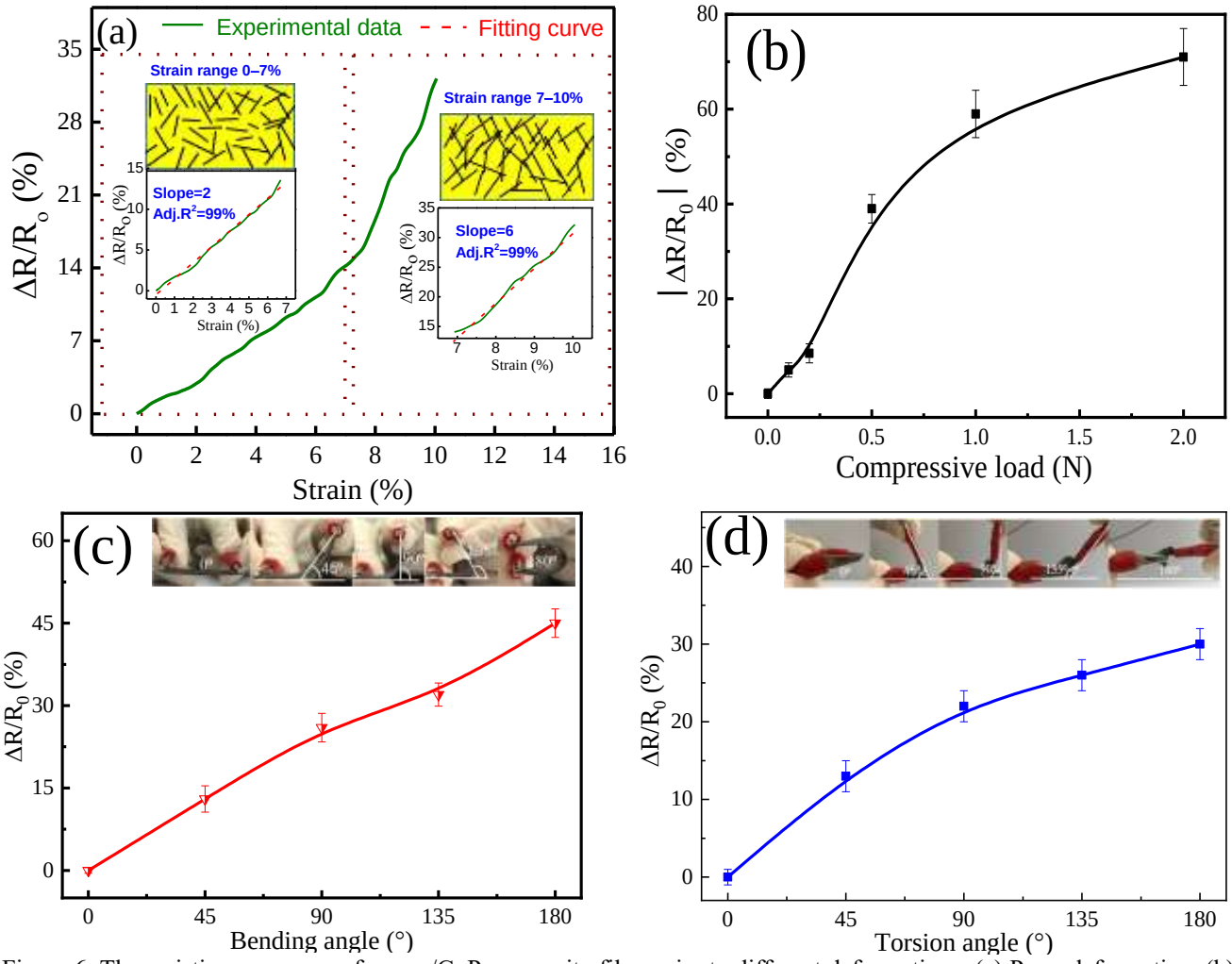

Figure 6. The resistive responses of epoxy/GnP composite films wire to different deformations: (a) Press deformation, (b) Bending deformation, (c) Torsional deformation, and (d) Tensile deformation.

3.5 Temperature Effect

Temperature is one of the most commonly sensed parameters due to the numerous of applications where knowing and using the actual or relative temperature is critical. Of most of signals, temperature monitoring is imperative in many physical, electronic, chemical, mechanical and biological systems [52-54]. The signal in temperature sensors is provided by a sudden increase or decrease in resistivity or capacitance with the temperature indicated by a positive or negative temperature coefficient [55]. Figure 7 shows the response of the composite film as a function of temperature.

Figure 7a presents the overall change in relative resistance of the composite film within the temperature range 20–110℃. It is noted that relative resistance change is linearly change with temperature within the specified range. The adjusted regression coefficient is 99%, which justifies that the linear regression is well fit and accurate with minimum offset points. The slope of the linear fit represents the temperature sensitivity (α) of the film according to Eq.5 [56]

$$\alpha = \frac{\Delta R}{R_o} \times \frac{1}{\Delta T} \qquad \text{Eq.5}$$

In temperature range 20–110℃, the temperature sensitivity is calculated as 0.63% (0.0063℃$^{-1}$) which is much higher than the standard commercial platinum-based temperature sensor (0.0039℃$^{-1}$) [56, 57]revealing that our film possess outstanding temperature sensing performance.

In order to test the stability and reliability of the developed film as a temperature sensor within range 20–110ºC, cyclic thermal test was carried out for a total of 40 cycles (Figure 7b and c). Initially, the relative resistance change is slowly decreasing until it stabilizes with increasing number of cycles. *Also, the film response at the first 5 cycles and last 5 cycles are compared (Figure 7c inset). It is observed that the relative resistance change of first 5 cycles is decreasing and not consistent with the steady state of the sensor revealing that the film is initially unstable till it passes the settle-in phase of a new sensor upon being newly manufactured. On the other hand, the relative resistance change in the last 5 cycles has reached a steady state response indicating a stable behavior as temperature sensor.*

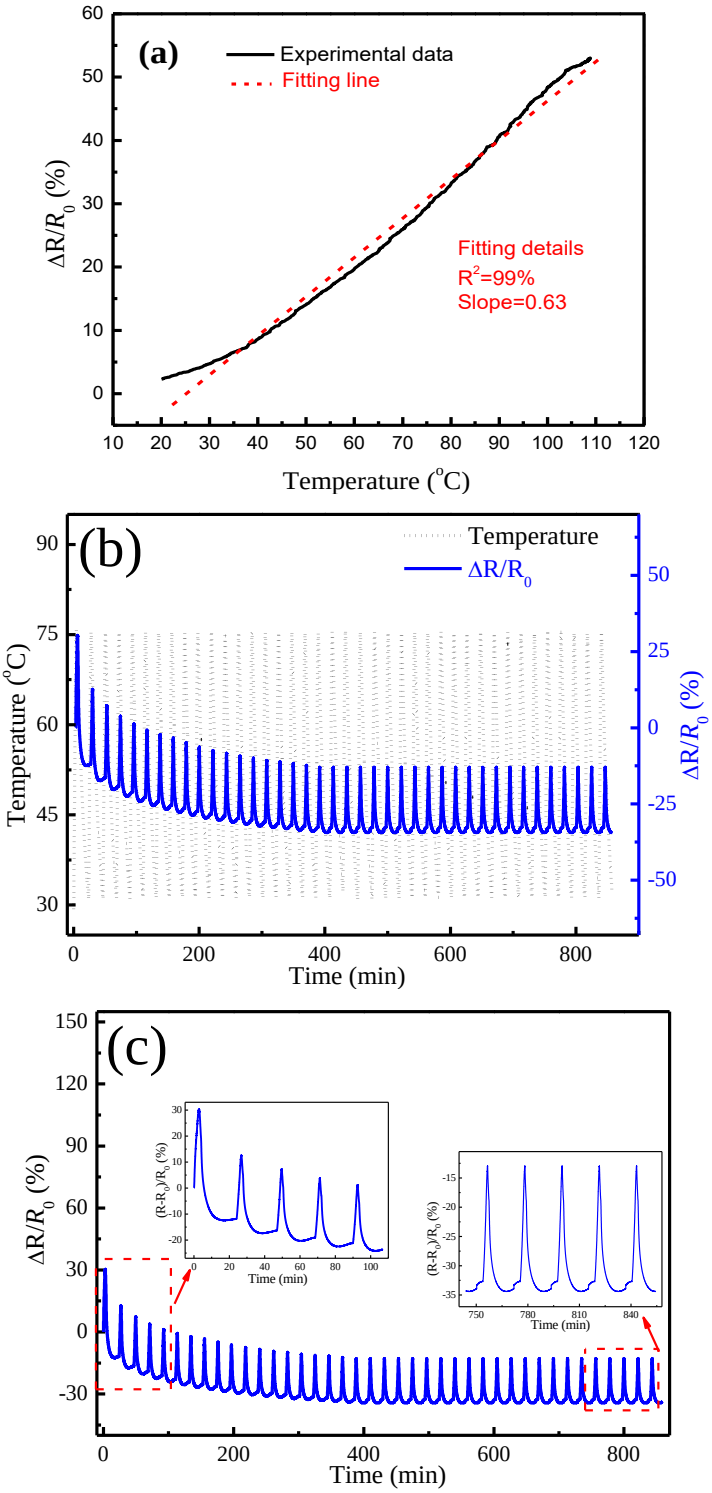

Figure 7. (a) The electric resistance response of epoxy/GnP composite film (10 vol%) during heating; (b) reliability of the composite film as thermal sensor within temperature range 30–75 °C for 40 cycle; and (c) comparison between first and last five thermal cycles

3.6 Fatigue Testing

Reliability represents how consistently a strain sensor can perform normal function without degradation, upon repeating it number of times. The cyclic tensile test was conducted to study the stability and durability of the composite film as a strain sensor. *Since the developed epoxy/GnP composite film is proposed to detect structure health monitoring, low strain and frequency were applied during the fatigue test [58-60].* The epoxy/GnP composite film (at 10 vol%) was tested for 10×10^3 cycles under 5% strain at 1Hz frequency, as shown in Figure 8a. Figures 8b–d are magnifications for composite film responses within the ranges of 0–1000, 4500–5500 and 9×10^3–10×10^3 cycles, respectively. *The relative resistance change ($\Delta R/R_0$) at first and last 10 cycles were compared (Figures 7b–d insets) in each range. In Figure 8b, the* epoxy/composite film demonstrates high consistency at the first and last 10 cycles revealing the resilience and repeatability of the film as a strain sensor.

On the other hand, the insets of Figure 8c shows a weak degeneration after 6000 cycles; upon unloading, the resistance change decreased to 2.3% instead of 0 as in Figure 7b. The observed degeneration is progressed and amplified in the last 1000 cycles (within range 9×10^3–10×10^3 cycles) as seen Figure 7d; when the load was released, the resistance change maintained 4% instead of getting back to zero. This zero-drift error is due to two main reasons: (i) the irreversible destruction of the GnP conductive networks caused by accumulation of microcracks and further yielding of the film due to fatigue damage, and (ii) the deterioration at the interface between the nanofiller and matrix upon cyclic loading [61]. This concludes that our epoxy/GnP composite film has high repeatability and resilience up to 5500 cycles.

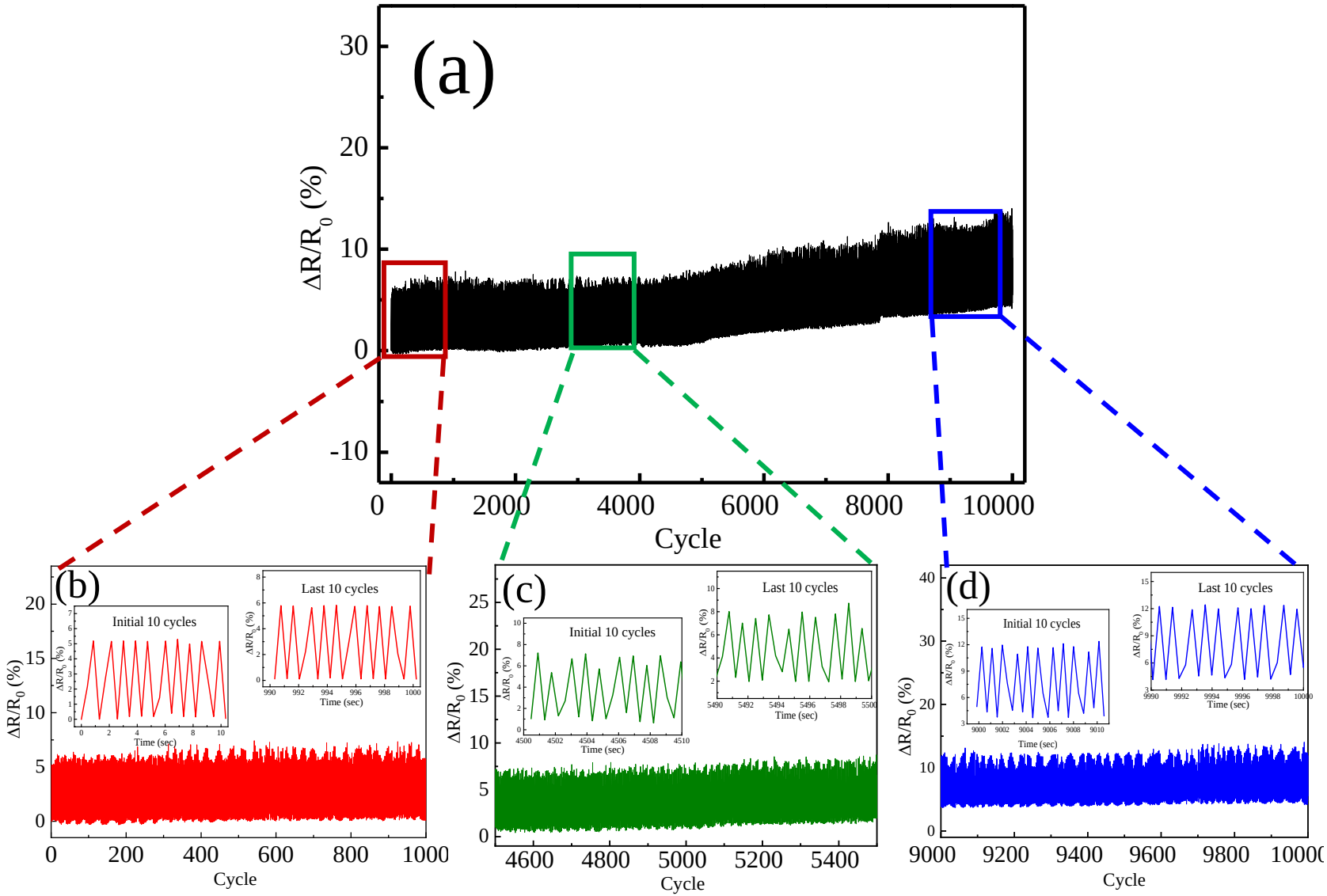

Figure 8. The cyclic tensile test of epoxy/GnP composite films at 5% strain and 1Hz, (a) the overall cyclic test over 10000 cycles, (b–d) magnifications of composite film responses within ranges of 0–1000, 4500–5500 and 9000–10000 cycles, respectively.

Conclusion

In this work, a durable, mechanically and thermally stable piezoresistive graphene-based film sensor was fabricated. Their microstructure and piezoresistive properties were investigated. At 10 vol% GnPs, Young's modulus and tensile strength of the composite film are 26 MPa and 1.0 MPa, recording 1344% and 66.7% improvement respectively. The percolation threshold of epoxy/GnPs composite film is observed at ~1.08 vol% of GnPs breaking the electrically nonconductive nature of the epoxy matrix. The thermal conductivity of composite film also showed prominent increase from 0.16 to 1.47 W m^{-1} K^{-1} reporting 818% improvement.

The epoxy/GnP film showed a good pressure response up to 2N, by demonstrating a 71% reduction in resistance. Furthermore, the flexible composite films demonstrated an excellent reliability and durability up to 5500 cycles with minimum zero-point drift and also proven to be responsive to bending and torsional angles up to 180°. Within the temperature range 20–110°C, the film demonstrated an excellent sensitivity to temperature change recording temperature sensitivity coefficient of 0.0063°C^{-1} which is far higher than the standard commercial temperature sensor (0.0039°C^{-1}).

Overall, this multifunctional composite film possesses substantial improvements in mechanical, electrical and thermal properties upon adding graphene platelets leading to outstanding piezoresistive performance under various mechanical and thermal loads. The composite film has the potential to work as a fully-fledged sensor in various engineering applications where temperature and mechanical loads require monitoring.

Acknowledgments

QM thanks Asbury (*Asbury, NJ, USA*) for providing the graphite intercalation compounds (1721). This work was financially supported by the Natural Science Foundation of Liaoning Province-China (20170520142 and 2019-MS-256), Aeronautical Science Foundation of China (2018ZF54036X),

China Postdoctoral Science Foundation (2019M651151) and National Natural Science Foundation (51973123).

Reference

1. Shi, G., et al., *Highly Sensitive, Wearable, Durable Strain Sensors and Stretchable Conductors Using Graphene/Silicon Rubber Composites.* Advanced Functional Materials, 2016. **26**(42): p. 7614-7625.
2. Zhang, B.-X., et al., *Multi-dimensional flexible reduced graphene oxide/polymer sponges for multiple forms of strain sensors.* Carbon, 2017. **125**: p. 199-206.
3. Aguilar Ventura, I., J. Zhou, and G. Lubineau, *Drastic modification of the piezoresistive behavior of polymer nanocomposites by using conductive polymer coatings.* Composites Science and Technology, 2015. **117**: p. 342-350.
4. Zhang, R.-C., et al., *Gold nanoparticle-polymer nanocomposites synthesized by room temperature atmospheric pressure plasma and their potential for fuel cell electrocatalytic application.* Scientific Reports, 2017. **7**: p. 46682.
5. Hicks, J.F., Y. Seok-Shon, and R.W. Murray, *Layer-by-Layer Growth of Polymer/Nanoparticle Films Containing Monolayer-Protected Gold Clusters.* Langmuir, 2002. **18**(6): p. 2288-2294.
6. Zhang, W., et al., *Conducting polymer/silver nanowires stacking composite films for high-performance electrochromic devices.* Solar Energy Materials and Solar Cells, 2019. **200**: p. 109919.
7. Shi, G., et al., *Facile Fabrication of Graphene Membranes with Readily Tunable Structures.* ACS Applied Materials & Interfaces, 2015. **7**(25): p. 13745-13757.
8. Ma, Q.M.H.-C.K.S.A.N.K.N.S.C.H.W.J., *Effect of interface modification on PMMA/graphene nanocomposites.*
9. Rahman, R. and P. Servati, *Effects of inter-tube distance and alignment on tunnelling resistance and strain sensitivity of nanotube/polymer composite films.* Nanotechnology, 2012. **23**(5): p. 055703.
10. Mo, L., et al., *Flexible transparent conductive films combining flexographic printed silver grids with CNT coating.* Nanotechnology, 2016. **27**(6): p. 065202.
11. Ha, J.U., et al., *Polyvinyl alcohol covalently grafted CNT for free-standing, flexible, and high-performance thermoelectric generator film.* Nanotechnology, 2019. **30**(14): p. 14LT01.
12. Zhang, Q., et al., *Conductive mechanism of carbon black/polyimide composite films*, in *Journal of Polymer Engineering*. 2018. p. 147.
13. Chun, K.Y., et al., *Highly conductive, printable and stretchable composite films of carbon nanotubes and silver.* Nature Nanotechnology, 2010. **5**(12): p. 853-7.
14. Araby, S., et al., *Elastomeric composites based on carbon nanomaterials.* Nanotechnology, 2015. **26**(11): p. 112001.
15. Araby, S., et al., *Electrically and thermally conductive elastomer/graphene nanocomposites by solution mixing.* Polymer, 2014. **55**(1): p. 201-210.
16. Araby, S., et al., *A novel approach to electrically and thermally conductive elastomers using graphene.* Polymer, 2013. **54**(14): p. 3663-3670.
17. Zaman, I., et al., *A Facile Approach to Chemically Modified Graphene and its Polymer Nanocomposites.* Advanced Functional Materials, 2012. **22**(13): p. 2735-2743.
18. Meng, Q., et al., *Effect of interface modification on PMMA/graphene nanocomposites.* Journal of Materials Science, 2014. **49**(17): p. 5838-5849.
19. Amjadi, M., et al., *Stretchable, Skin-Mountable, and Wearable Strain Sensors and Their Potential Applications: A Review.* 2016. **26**(11): p. 1678-1698.
20. Mora, A., F. Han, and G. Lubineau, *Estimating and understanding the efficiency of nanoparticles in enhancing the conductivity of carbon nanotube/polymer composites.* Results in Physics, 2018. **10**: p. 81-90.
21. Sun, Z., et al., *Growth of graphene from solid carbon sources.* Nature, 2010. **468**(7323): p. 549-552.
22. Wichmann, M.H.G., et al., *Piezoresistive response of epoxy composites with carbon nanoparticles under tensile load.* Physical Review B, 2009. **80**(24): p. 245437.
23. Bautista-Quijano, J.R., et al., *Strain sensing capabilities of a piezoresistive MWCNT-polysulfone film.* Sensors and Actuators A: Physical, 2010. **159**(2): p. 135-140.

24. *A Review: Carbon Nanotube-Based Piezoresistive Strain Sensors.* Journal of Sensors, 2012. **2012**: p. 15.
25. Gau, C., H.S. Ko, and H.T. Chen, *Piezoresistive characteristics of MWNT nanocomposites and fabrication as a polymer pressure sensor.* Nanotechnology, 2009. **20**(18): p. 185503.
26. Hamdi, K., et al., *Improvement of the electrical conductivity of carbon fiber reinforced polymer by incorporation of nanofillers and the resulting thermal and mechanical behavior.* Journal of Composite Materials, 2018. **52**(11): p. 1495-1503.
27. Lu, S., et al., *Strain sensing behaviors of GnPs/epoxy sensor and health monitoring for composite materials under monotonic tensile and cyclic deformation.* Composites Science and Technology, 2018. **158**: p. 94-100.
28. Wichmann, M.H., et al., *Piezoresistive response of epoxy composites with carbon nanoparticles under tensile load.* 2009. **80**(24): p. 245437.
29. Wang, X., et al., *Highly Stretchable and Wearable Strain Sensor Based on Printable Carbon Nanotube Layers/Polydimethylsiloxane Composites with Adjustable Sensitivity.* ACS Applied Materials & Interfaces, 2018. **10**(8): p. 7371-7380.
30. Collins, P.G., et al., *Extreme Oxygen Sensitivity of Electronic Properties of Carbon Nanotubes.* Science, 2000. **287**(5459): p. 1801.
31. Nela, L., et al., *Large-Area High-Performance Flexible Pressure Sensor with Carbon Nanotube Active Matrix for Electronic Skin.* Nano Letters, 2018. **18**(3): p. 2054-2059.
32. Liu, Y., et al., *Room Temperature Broadband Infrared Carbon Nanotube Photodetector with High Detectivity and Stability.* 2016. **4**(2): p. 238-245.
33. Zha, J.-W., et al., *High-performance strain sensors based on functionalized graphene nanoplates for damage monitoring.* Composites Science and Technology, 2016. **123**: p. 32-38.
34. Chun, S., Y. Choi, and W. Park, *All-graphene strain sensor on soft substrate.* Carbon, 2017. **116**: p. 753-759.
35. Zaman, I.K., H. C. Dai, J. Kawashima, N. Michelmore, A. Sovi, A. Dong, S. Luong, L. Ma, J., *From carbon nanotubes and silicate layers to graphene platelets for polymer nanocomposites.* Nanoscale, 2012. **4**(15): p. 4578-86.
36. Araby, S., et al., *Melt compounding with graphene to develop functional, high-performance elastomers.* Nanotechnology, 2013. **24**(16): p. 165601.
37. Zaman, I., et al., *From carbon nanotubes and silicate layers to graphene platelets for polymer nanocomposites.* Nanoscale, 2012. **4**(15): p. 4578-4586.
38. Meng, Q., et al., *Free-standing, flexible, electrically conductive epoxy/graphene composite films.* Composites Part A: Applied Science and Manufacturing, 2017. **92**: p. 42-50.
39. Pei, S. and H.-M. Cheng, *The reduction of graphene oxide.* Carbon, 2012. **50**(9): p. 3210-3228.
40. Ferrari, A.C. and D.M. Basko, *Raman spectroscopy as a versatile tool for studying the properties of graphene.* Nature Nanotechnology, 2013. **8**: p. 235.
41. Malard, L.M., et al., *Raman spectroscopy in graphene.* Physics Reports, 2009. **473**(5): p. 51-87.
42. Zaman, I., et al., *From carbon nanotubes and silicate layers to graphene platelets for polymer nanocomposites.* Nanoscale, 2012. **4**(15): p. 4578-4586.
43. Wu, Z.-S., et al., *Synthesis of Graphene Sheets with High Electrical Conductivity and Good Thermal Stability by Hydrogen Arc Discharge Exfoliation.* ACS Nano, 2009. **3**(2): p. 411-417.
44. Marcano, D.C., et al., *Improved Synthesis of Graphene Oxide.* Acs Nano, 2010. **4**(8): p. 4806-4814.
45. Stankovich, S., et al., *Graphene-based composite materials.* Nature, 2006. **442**(7100): p. 282-286.
46. Su, Y., J.J. Li, and G.J. Weng, *Theory of thermal conductivity of graphene-polymer nanocomposites with interfacial Kapitza resistance and graphene-graphene contact resistance.* Carbon, 2018. **137**: p. 222-233.
47. Han, Z. and A. Fina, *Thermal conductivity of carbon nanotubes and their polymer nanocomposites: a review.* Progress in polymer science, 2011. **36**(7): p. 914-944.
48. Chen, Y., et al., *Advances in graphene-based polymer composites with high thermal conductivity.* Veruscript Functional Nanomaterials, 2018. **2**: p. oosb06.
49. Meng, Q., et al., *Mechanically robust, electrically and thermally conductive graphene-based epoxy adhesives.* Journal of Adhesion Science and Technology, 2019. **33**(12): p. 1337-1356.
50. Ma, J., et al., *Development of polymer composites using modified, high-structural integrity graphene platelets.* Composites Science and Technology, 2014. **91**: p. 82-90.
51. Kuan, H.-C., J.-B. Dai, and J. Ma, *A reactive polymer for toughening epoxy resin.* Journal of Applied

Polymer Science, 2010. **115**(6): p. 3265-3272.
52. Kunzelman, J., et al., *Shape memory polymers with built-in threshold temperature sensors.* Journal of Materials Chemistry, 2008. **18**(10): p. 1082-1086.
53. Mohiuddin, M., et al., *Flexible cellulose acetate/graphene blueprints for vibrotactile actuator.* RSC Advances, 2015. **5**(43): p. 34432-34438.
54. Robinson, J.T., et al., *Reduced Graphene Oxide Molecular Sensors.* Nano Letters, 2008. **8**(10): p. 3137-3140.
55. Al-Mumen, H., et al., *Thermo-flow and temperature sensing behaviour of graphene based on surface heat convection.* Iet Micro & Nano Letters, 2013. **8**(10): p. 681-685.
56. Wang, Z., et al., *3D-Printed Graphene/Polydimethylsiloxane Composites for Stretchable and Strain-Insensitive Temperature Sensors.* ACS Applied Materials & Interfaces, 2019. **11**(1): p. 1344-1352.
57. Kuo, J.T.W., L. Yu, and E. Meng, *Micromachined Thermal Flow Sensors—A Review.* Micromachines, 2012. **3**(3): p. 550-573.
58. Tung, T.T., et al., *Engineering of graphene/epoxy nanocomposites with improved distribution of graphene nanosheets for advanced piezo-resistive mechanical sensing.* Journal of Materials Chemistry C, 2016. **4**(16): p. 3422-3430.
59. Moriche, R., et al., *Strain monitoring mechanisms of sensors based on the addition of graphene nanoplatelets into an epoxy matrix.* Composites Science and Technology, 2016. **123**: p. 65-70.
60. Eswaraiah, V., K. Balasubramaniam, and S. Ramaprabhu, *Functionalized graphene reinforced thermoplastic nanocomposites as strain sensors in structural health monitoring.* Journal of Materials Chemistry, 2011. **21**(34): p. 12626-12628.
61. Qiu, A., et al., *A Path Beyond Metal and Silicon:Polymer/Nanomaterial Composites for Stretchable Strain Sensors.* 2019. **29**(17): p. 1806306.